Improvement of reverse blocking performance in vertical power MOSFETs with Schottky–drain-connected semisuperjunctions*

Wei Mao(毛维)[1], Hai-Yong Wang(王海永)[1], Xiao-Fei Wang(王晓飞)[2,†], Ming Du(杜鸣)[1], Jin-Feng Zhang(张金凤)[1], Xue-Feng Zheng(郑雪峰)[1], Chong Wang(王冲)[1], Xiao-Hua Ma(马晓华)[1], Jin-Cheng Zhang(张进成)[1], and Yue Hao(郝跃)[1]

[1] *Key Laboratory of the Ministry of Education for Wide Band-Gap Semiconductor Materials and Devices, School of Microelectronics, Xidian University, Xi'an* 710071, *China*

[2] *Xian Aerosemi Technology Co., LTD, Xi'an* 710077, *China*

(Received 14 December 2016; revised manuscript received 3 February 2017; published online 10 March 2017)

To enhance the reverse blocking capability with low specific on-resistance, a novel vertical metal–oxide–semiconductor field-effect transistor (MOSFET) with a Schottky–drian (SD) and SD-connected semisuperjunctions (SD-D-semi-SJ), named as SD-D-semi-SJ MOSFET is proposed and demonstrated by two-dimensional (2D) numerical simulations. The SD contacted with the n-pillar exhibits the Schottky-contact property, and that with the p-pillar the Ohmic-contact property. Based on these features, the SD-D-semi-SJ MOSFET could obviously overcome the great obstacle of the ineffectivity of the conventional superjunctions (SJ) or semisuperjunctions (semi-SJ) for the reverse applications and achieve a satisfactory trade-off between the reverse breakdown voltage (BV) and the specific on-resistance ($R_{on}A$). For a given pillar width and n-drift thickness, there exists a proper range of n-drift concentration (N), in which the SD-D-semi-SJ MOSFET could exhibit a better trade-off of $R_{on}A$–BV compared to the predication of SJ MOSFET in the forward applications. And what is much valuable, in this proper range of N, the desired BV and good trade-off could be achieved only by determining the pillar thickness, with the top assist layer thickness unchanged. Detailed analyses have been carried out to get physical insights into the intrinsic mechanism of $R_{on}A$–BV improvement in SD-D-semi-SJ MOSFET. These results demonstrate a great potential of SD-D-semi-SJ MOSFET in reverse applications.

Keywords: vertical MOSFET, Schottky–drain-connected semisuperjunction (SD-D-semi-SJ), reverse blocking, specific on-resistance

PACS: 73.40.Qv, 85.30.Tv, 85.30.De **DOI:** 10.1088/1674-1056/26/4/047306

1. Introduction

As the core component, power MOSFETs have been playing more and more important roles in many power electronics, such as automotive electronics, inverter systems and power switches. So far, many studies have been performed to improve the performance of MOSFETs, of which the introduction of the superjunction (SJ) into vertical MOSFETs, as a milestone in the development of MOSFETs, has been a prominent catalyst for improving the power performance.[1] And the MOSFETs with SJ, named as SJ MOSFETs, have opened up important opportunities for breaking the silicon limit of power MOSFETs, which have attracted much attention in the optimization of SJ structure and the development of novel SJ MOSFETs structures.[2–12] Moreover, the explorations of SJ MOSFETs structures and mechanisms are still on the road.

Recently, actual demands in power converters,[13] class-S amplifier,[14] and power management systems[15,16] stimulate many researchers to put the focus on the development of Schottky–drain (SD) lateral devices with a good reverse blocking capability,[17–19] namely the drain electrode of devices may undergo a great negative bias at the off-state. This could provide a good deal of significant enlightenment that if it is possible to realize the desired reverse blocking ability based on the vertical MOSFET with a SD (SD MOSFET), the SJ MOSFET with a SD (SD-SJ MOSFET) or semisuperjunction MOSFET (semi-SJ MOSFET[3]) with an SD (SD-semi-SJ MOSFET). Unfortunately, so far, none of studies about these has been reported. And what is worse, it is nearly ineffective to enhance the reverse blocking capability with SD-SJ MOSFETs or SD-semi-SJ MOSFETs according to our studies in this paper.

In this paper, for the first time, a novel vertical SD-D-semi-SJ MOSFET with a high workfunction SD and SD-connected semisuperjunctions is proposed for the purpose of excellent reverse breakdown voltage (BV) and low specific on-resistance ($R_{on}A$). The SD contacted with the p-pillar or the n-pillar shows an Ohimc contact performance or a Schottky contact performance, respectively. These features could overcome the drawback of conventional devices during the reverse appli-

*Project supported by the National Natural Science Foundation of China (Grant Nos. 61574112, 61334002, 61306017, 61474091, and 61574110) and the Natural Science Basic Research Plan in Shaanxi Province of China (Grant No. 605119425012).

†Corresponding author. E-mail: xjtuwxf@126.com

© 2017 Chinese Physical Society and IOP Publishing Ltd

cations. Systematic and comparative studies of the proposed SD-D-semi-SJ MOSFET, related to the device physical mechanisms, the device optimization as well as the trade-off property, have been performed based on two-dimensional numerical simulations with Silvaco-Atlas.[20] And the device fabrication issues are also discussed. These results demonstrate feasible reverse applications of the SD-D-semi-SJ MOSFET.

2. Device structures

The cross section schematics of the SD MOSFET, the SD-semi-SJ MOSFET and the proposed SD-D-semi-SJ MOSFET are shown in Fig. 1. The SD-D-semi-SJ structure is composed of the SD-connected semi-SJ structure combined with top assist layer (TAL) while the SD-semi-SJ structure the body-connected semi-SJ combined with bottom assist layer (BAL). All the devices have the same main dimensions as shown in Table 1, unless otherwise stated. The same concentration N is used in n-drift layer, n-pillar, p-pillar, TAL, and BAL for all devices. The Schottky–drain contact with a workfunction of 5 eV is used. It is worth noting that SD contacted with the n-pillar (and the n-drift) or the p-pillar could be considered as the Schottky-contact property or the Ohmic-contact property, respectively, due to the electron affinity of about 4.05 eV in silicon.

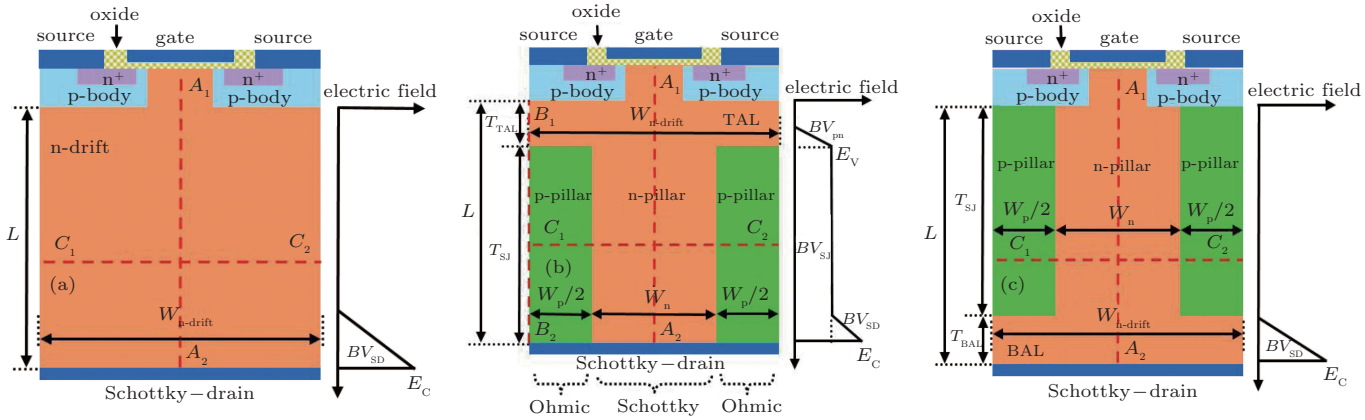


Fig. 1. (color online) Cross section schematics and electric field distribution sketch along the line A_1A_2 for (a) SD MOSFET, (b) SD-D-semi-SJ MOSFET, and (c) SD-semi-SJ MOSFET. The line A_1A_2 or B_1B_2 denotes the vertical direction at the middle or the left edge of device, respectively. The line C_1C_2 denotes the horizontal direction at a distance of 14 μm from the Schottky–drain.

Table 1. Device specifications.

Symbol	Description	Values
L/μm	n-drift thickness	35
$W_{n-drift}$/μm	n-drift width	16
W_n/μm	n-pillar width	8
W_p/μm	p-pillar width	8
	n-drift doping concentration	
N/cm^{-3}	n-pillar doping concentration	7×10^{15}
	p-pillar doping concentration	
A/μm^2	active region area	16
T_{TAL}	top assist layer thickness	–
T_{BAL}	bottom assist layer thickness	–
T_{SJ}	SJ thickness	–

3. On-state and off-state analyses

3.1. On-state performance

Figure 2 shows the I–V curves of the on-state performance at V_{GS} = 10 V and V_{DS} = 30 V for the SD MOSFET, the SD-D-semi-SJ MOSFET, and the SD-semi-SJ MOSFET. A slight onset voltage of 0.5 V (at the drain current of 10^{-6} A/μm[17]) could be seen for all the devices, which is introduced by the Schottky barrier. And it is amazing that the current of the SD-D-semi-SJ MOSFET is obviously greater than other two devices at the same V_{DS}, leading to the smallest $R_{SD-D-semi-SJ}A$ of 6.6 mΩ·cm^2. The lowest current and the biggest $R_{SD-semi-SJ}A$ of 17 mΩ·cm^2 appear in the SD-semi-SJ MOSFET. In order to reveal the physical mechanisms of these phenomena, figure 3 shows the two-dimensional (2D) current density distributions. Because the obvious differences between the three devices in Fig. 3 lie in the connection manner of the p-pillar.

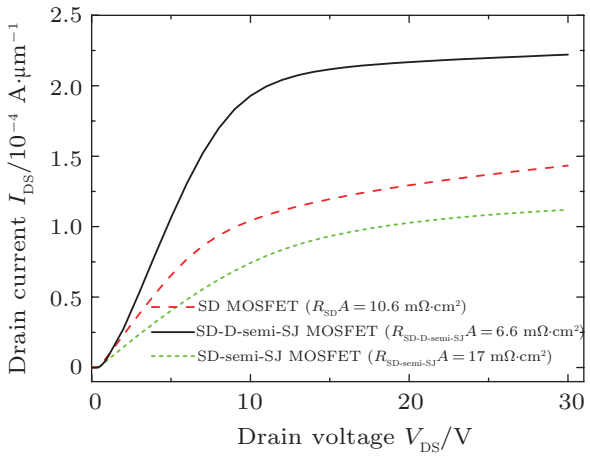


Fig. 2. (color online) I–V curves of on-state at V_{GS} = 10 V for three devices. $N = 3\times10^{15}$ cm^{-3}, $W_n = W_p$ = 8 μm, $W_{n-drift}$ = 16 μm for all devices. $T_{TAL} = T_{BAL}$ = 7 μm.

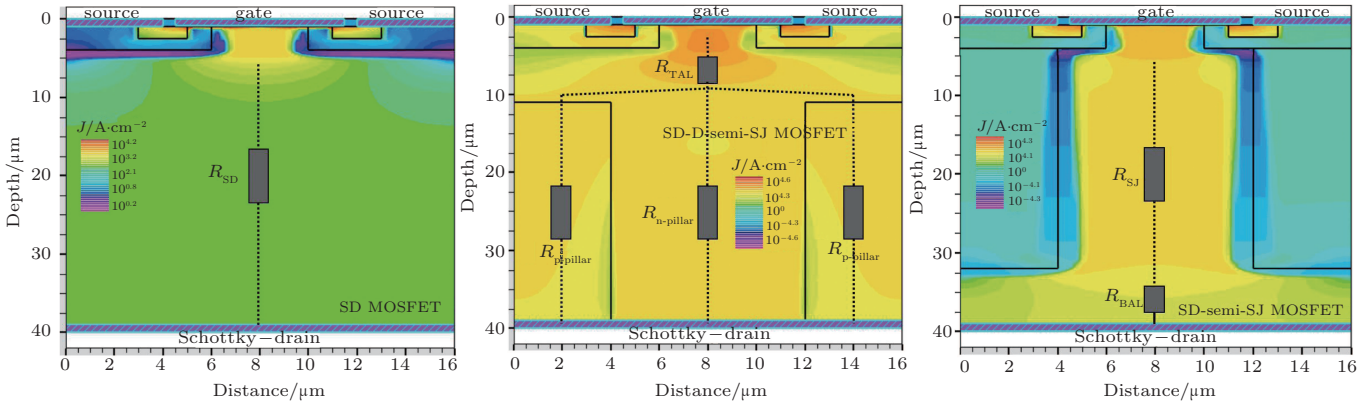


Fig. 3. (color online) The 2D current density distributions at $V_{GS} = 10$ V and $V_{DS} = 5$ V corresponding to the devices in Fig. 2.

Figure 4 gives the one-dimensional (1D) current density distributions along the line C_1C_2 as shown in Fig. 1. Based on Figs. 3 and 4, it could be seen that the currents in both SD MOSFET and SD-semi-SJ MOSFET are mostly composed of electron current. Only the n-pillar and the bottom n-drift layer could effectively conduct current in SD-semi-SJ MOSFET. In contrast, for SD-D-semi-SJ MOSFET, both the n-pillar and the p-pillar could conduct current, whose current then could be collected by the TAL beneath the gate. Careful analysis shows the junction between the p-pillar and the TAL remains forward biased. Therefore, in SD-D-semi-SJ MOSFET, the current conducted through the p-pillar is composed of both the electron and the hole current while that through the n-pillar the electron current as illustrated in Fig. 4.

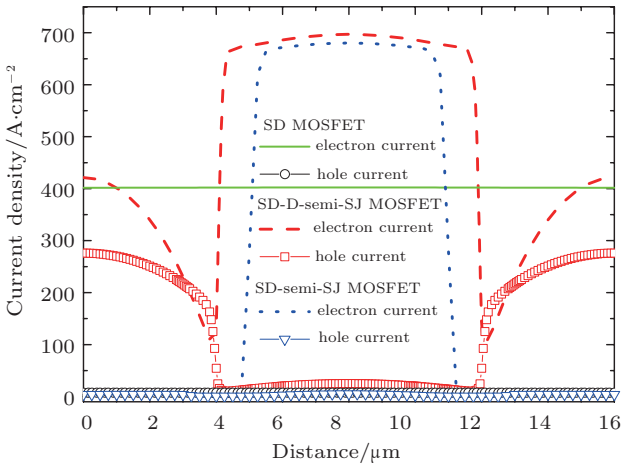


Fig. 4. (color online) Current density distributions along the line C_1C_2 as shown in Fig. 1 corresponding to the devices in Fig. 3.

In Fig. 4, in comparison with the SD MOSFET, although the current density in the n-pillar in the SD-semi-SJ MOSFET is increased by about 70%, the current density in other parts is much small. This leads to a greater $R_{on}A$ in the SD-semi-SJ MOSFET in comparison with the SD MOSFET. For the SD-D-semi-SJ MOSFET, the current density in the n-pillar is much greater than that in the SD MOSFET. And both the electron current and hole current with high density could be seen in the p-pillar in the SD-D-semi-SJ MOSFET, which could result in a greater total current density in the p-pillar in comparison with the SD MOSFET. Thus, it could be predicted that the SD-D-semi-SJ MOSFET could obtain the smaller $R_{on}A$ than the SD MOSFET.

According to these analyses mentioned above, the specific on-resistance for the three devices in Fig. 3 could be deduced approximately. For the SD MOSFET,

$$R_{SD}A = \frac{L}{q\mu_n N}, \tag{1}$$

where q is an electron charge, and μ_n is electron mobility. For the SD-semi-SJ MOSFET,

$$\begin{aligned} R_{SD-semi-SJ}A &= R_{BAL}A + R_{SJ}A \\ &= \frac{T_{BAL}}{q\mu_n N} + \frac{2T_{SJ}}{q\mu_n N} = \frac{L + T_{SJ}}{q\mu_n N}, \end{aligned} \tag{2}$$

where R_{BAL} and R_{SJ} are the resistance related to the BAL and the n-pillar, respectively. And for the SD-D-semi-SJ MOSFET,

$$\begin{aligned} R_{SD-D-semi-SJ}A &= R_{SJ}A + R_{TAL}A \\ &= \left(R_{n-pillar} \parallel \frac{R_{p-pillar}}{2}\right)A + R_{TAL}A \\ &= \left(\frac{2T_{SJ}}{q\mu_n N} \parallel \frac{2T_{SJ}}{q(\mu_n + \mu_p)N}\right) + \frac{T_{TAL}}{q\mu_n N} \\ &= \frac{2T_{SJ}}{q(2\mu_n + \mu_p)N} + \frac{T_{TAL}}{q\mu_n N}, \end{aligned} \tag{3}$$

where $R_{n-pillar}$ and $R_{p-pillar}$ are the resistances related to the n-pillar and the p-pillar, respectively, μ_p is the hole mobility, and R_{SJ} is the equivalent resistance of $R_{n-pillar}$ in parallel with $R_{p-pillar}$. Therefore, it is clear that $R_{SD-D-semi-SJ} < R_{SD} < R_{SD-semi-SJ}$ because of $\mu_n \approx 3\mu_p$, which is consistent with the results in Fig. 2. This further demonstrates a remarkable advantage of on-state performance of the SD-D-semi-SJ MOSFET.

3.2. Off-state performance

The off-state I–V performance is depicted in Fig. 5.

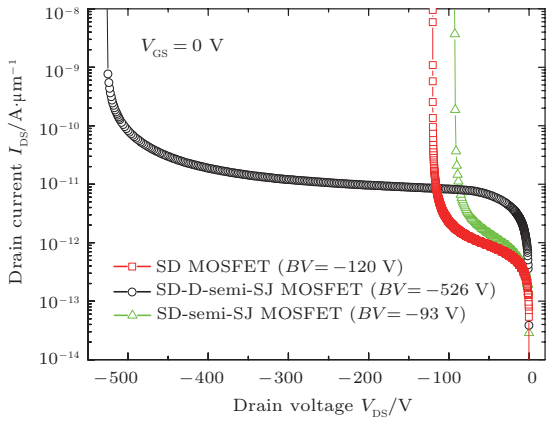


Fig. 5. (color online) The off-state I–V performance corresponding to the devices in Fig. 2.

Based on Fig. 2 and Fig. 5, the SD-D-semi-SJ MOSFET shows the excellent reverse blocking capability ($BV_{SD-D-semi-SJ} = -526$ V) as well as on-state performance ($R_{SD-D-semi-SJ}A = 6.6$ mΩ · cm^2), compared with the SD MOSFET ($BV_{SD} = -120$ V and $R_{SD}A = 10.6$ mΩ · cm^2) and the SD-semi-SJ MOSFET ($BV_{SD-semi-SJ} = -93$ V and $R_{SD-semi-SJ}A = 17$ mΩ · cm^2). Clear physical understanding of the intrinsic mechanism related to the blocking improvement above could be achieved based on Fig. 6, Fig. 7, and the electric field distribution sketch in Fig. 1. As can be seen, the high equipotential lines density regions, namely the depletion regions, are only near the Schottky–drain in both the SD MOSFET and the SD-semi-SJ MOSFET, due to the reverse biased SD/n-drift (or SD/BAL) diode. Thus, for the SD MOSFET the absolute value of the reverse breakdown voltage could be estimated by

$$BV_{SD} = \frac{W_{SD}E_C}{2} = \frac{E_C^2\varepsilon}{2qN}, \tag{4}$$

where W_{SD} is the depletion region thickness of the SD/n-drift junction, E_C is the critical electric field, and ε is the dielectric constant.

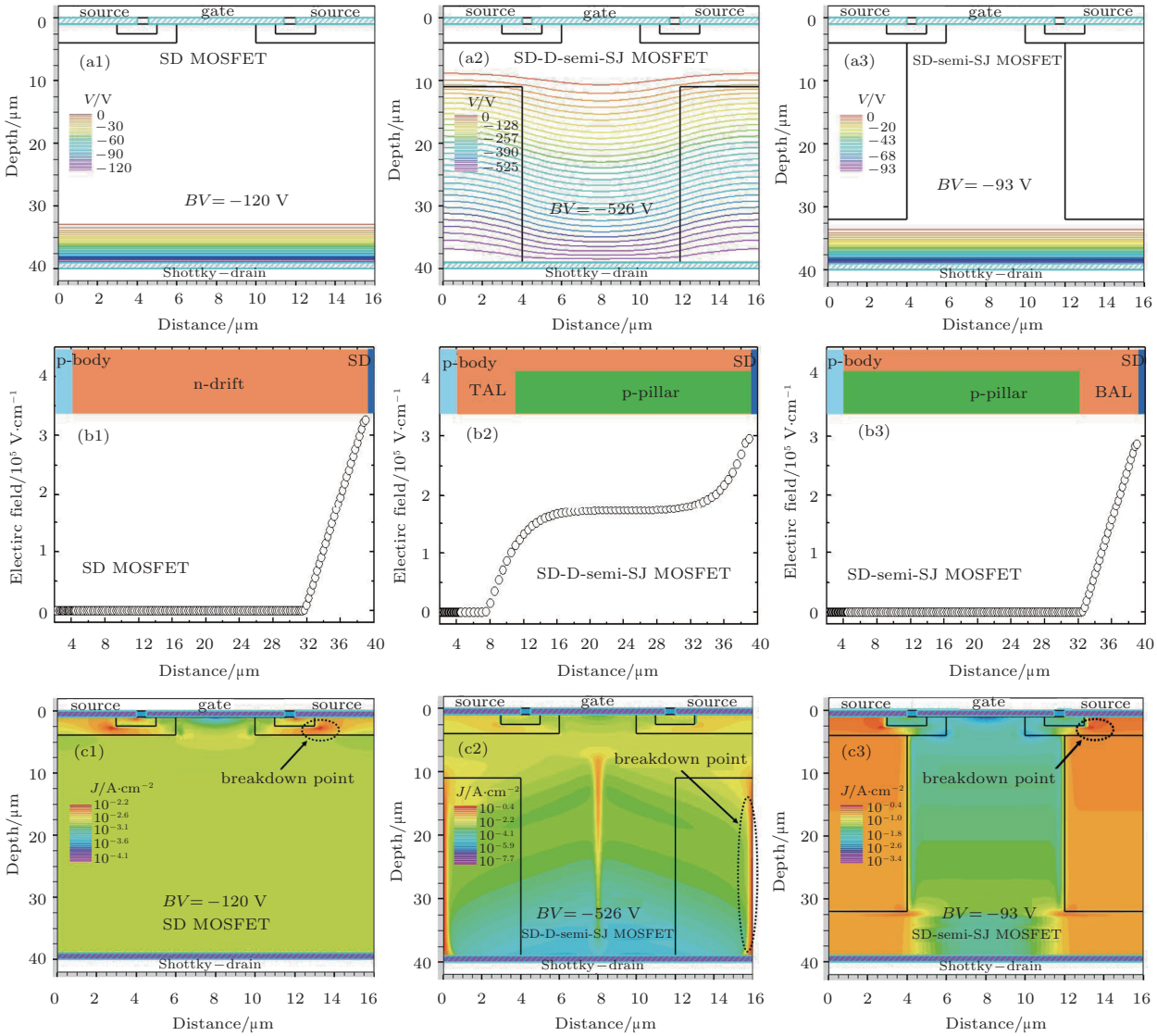


Fig. 6. (color online) Off-state performances at reverse BV in three devices corresponding to Fig. 5: (a) equipotential lines distribution, (b) electric field distribution along the line A_1A_2 as shown in Fig. 1, and (c) total current density distribution. $N = 3 \times 10^{15}$ cm^{-3}, $W_n = W_p = 8$ μm, $W_{n-drift} = 16$ μm for all devices. $T_{TAL} = T_{BAL} = 7$ μm.

For the SD-semi-SJ MOSFET, only the BAL rather than the SJ layer could sustain the reverse blocking. Thus, when its T_{BAL} is smaller than the W_{SD} of the SD MOSFET, adopting the T_{BAL} instead of W_{SD} as the depletion region thickness approximately, its absolute BV could be estimated by

$$BV_{SD-semi-SJ} = \frac{T_{BAL}E_C}{2}. \quad (5)$$

And the $BV_{SD-semi-SJ}$ will increase slightly with the increasing T_{BAL}, until the $BV_{SD-semi-SJ}$ approaches the BV_{SD} when $T_{BAL} \geqslant W_{SD}$.

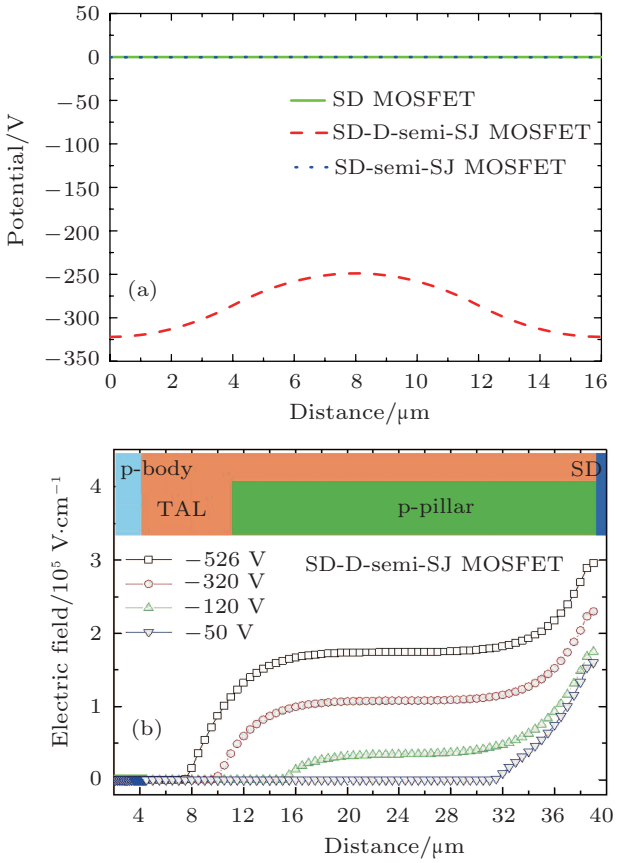


Fig. 7. (color online) (a) Potential distributions along the line C_1C_2 as shown in Fig. 1 corresponding to the devices in Fig. 6(a), and (b) electric field distribution along the line A_1A_2 in the SD-D-semi-SJ MOSFET for different Schottky–drain bias voltages corresponding to Fig. 6(b).

For the SD-D-semi-SJ MOSFET, it could be observed from Fig. 7(a) that the potential in the n-pillar is higher than that in the p-pillar, which indicates the junction between the p-pillar and the n-pillar is under the reverse bias and could sustain the drain voltage. Therefore, a much broader and relatively more equal-spaced distribution of the equipotential lines could be obtained due to the adopted SD-D-semi-SJ, leading to a more uniform electric field distribution as shown in Fig. 6(b). In addition, as shown in Fig. 7(b), with the increase of the reverse drain bias, the Schottky–drain could first sustain the drain voltage, and then the n-pillar could gradually exhibit the effect on sustaining the drain voltage. Thus, the SD-D-semi-SJ MOSFET could withstand a greater breakdown voltage and its absolute BV could be estimated by

$$\begin{aligned} BV_{SD-D-semi-SJ} &= BV_{SD} + BV_{SJ} + BV_{pn} \\ &= \frac{\left(3-2\sqrt{2}\right)E_C^2\varepsilon}{4qN} + E_V T_{SJ} + \frac{\sqrt{2}E_C^2\varepsilon}{4qN} \\ &= \frac{E_C}{\sqrt{2}}T_{SJ} + \frac{\left(3-\sqrt{2}\right)E_C^2\varepsilon}{4qN}, \end{aligned} \quad (6)$$

where BV_{SD}, BV_{SJ}, and BV_{pn} are contributed by the SD/n-drift junction, the semisuperjunction, and the p-pillar/TAL junction, respectively. Assuming $T_{SJ} > W_N$ for simplicity, based on $E_V = E_C/\sqrt{2} = qNW_n/2\varepsilon$,[3] then the theoretical estimation results, $BV_{SD-D-semi-SJ} > BV_{SD} > BV_{SD-semi-SJ}$, could be deduced, which are in agreement with simulation results in Fig. 5. Furthermore, from Fig. 6 it could also be seen that the dominant factor inducing device breakdown for the SD-D-semi-SJ MOSFET could be attributed to the high total current density regions near the two sides of the device while that for the SD MOSFET and the SD-semi-SJ MOSFET stem from the n^+/p-body junction. Besides, the SD-SJ MOSFET is also concerned. But this device shows a bad off-state performance, because the source and the drain are shorted together through the p-body and the p-pillar.

4. Optimization for maximum breakdown voltage

Figure 8 illustrates the BV and the $R_{on}A$ versus the n-drift concentration in the SD-MOSFET. Both the absolute BV and the $R_{on}A$ increase with the decreasing N, which is attributed to the depletion effect of the Schottky–drain/n-drift junction. This implies the N should be further reduced so as to enhance the BV at the expense of the $R_{on}A$. However, this bottleneck could be broken with the proposed SD-D-semi-SJ MOSFET, as shown in Section 3.

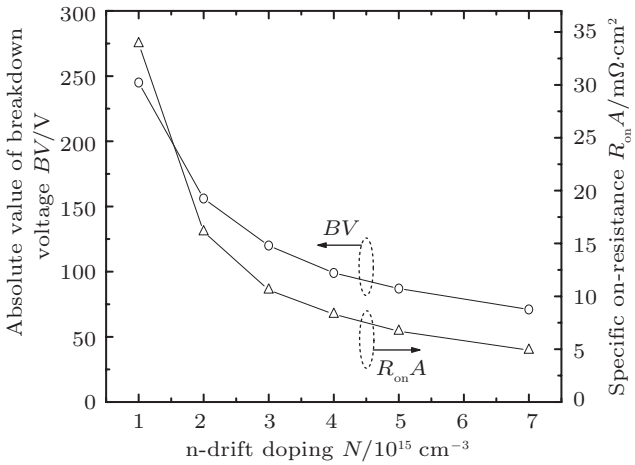


Fig. 8. The breakdown voltage and the specific on-state resistance versus the n-drift concentration in the SD MOSFET.

Figure 9 gives the relationship of the BV and the $R_{on}A$ versus the p-pillar height T_{SJ} in the SD-D-semi-SJ MOSFET.

As shown in the figure, due to the conduction of the p-pillar at on-state, the $R_{on}A$ is not sensitive to T_{SJ}. Thus, the small $R_{on}A$ with the range of 5.6 m$\Omega\cdot$cm^2 to 7.3 m$\Omega\cdot$cm^2 could be observed clearly. In contrast, the strong effect of T_{SJ} on BV could be seen, with the greatest absolute BV of 526 V at $T_{SJ} = 28$ μm.

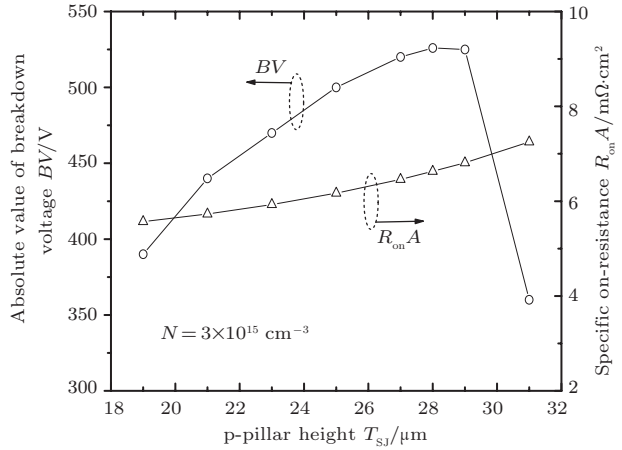


Fig. 9. The breakdown voltage and the specific on-state resistance versus the p-pillar height in the SD-D-semi-SJ MOSFET. $N = 3\times10^{15}$ cm^{-3}.

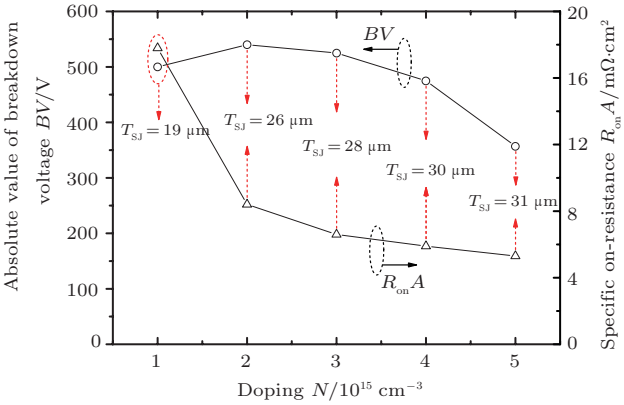


Fig. 10. (color online) The optimized breakdown voltage and the specific on-state resistance versus the n-drift concentration N in the SD-D-semi-SJ MOSFET. Each breakdown voltage is obtained by optimizing the p-pillar height T_{SJ} to approach the maximum value for a given N.

The relationship of the optimized BV and the $R_{on}A$ versus the N in the SD-D-semi-SJ MOSFET is illustrated in Fig. 10. The p-pillar height T_{SJ} is optimized in order to achieve the maximum BV for a given N. Comparing Fig. 8 with Fig. 10, it could be observed that although the $R_{on}A$ increases with the decreasing N in the SD-D-semi-SJ MOSFET, all the values of $R_{on}A$ are smaller than those in the SD MOSFET for the same N. Furthermore, the lower the N, the greater the difference of $R_{on}A$ between the SD-MOSFET and the SD-D-semi-SJ MOSFET. And for the given N all the BV in the SD-D-semi-SJ MOSFET are much greater than those in the SD-MOSFET. The peak absolute BV of 540 V with an $R_{on}A$ of 8.4 m$\Omega\cdot$cm^2 could be extracted for $N = 2\times10^{15}$ cm^{-3} and $T_{SJ} = 26$ μm in the SD-D-semi-SJ MOSFET. Those exhibit the superiority of the SD-D-semi-SJ MOSFET over the SD MOSFET.

During the optimization of the p-pillar height T_{SJ} for different N in the SD-D-semi-SJ MOSFET, it is also found that the BV is a weak dependence on T_{SJ} for the higher N, which deviates from the rules in Fig. 9. Figure 11 shows this relationship of BV and $R_{on}A$ versus T_{SJ} for $N = 7\times10^{15}$ cm^{-3}. The variation of $R_{on}A$ with T_{SJ} is similar to that in Fig. 9, of which extremely low $R_{on}A$ with the range of 3.2 m$\Omega\cdot$cm^2 to 4.6 m$\Omega\cdot$cm^2 could be obtained due to the high doping concentration. However, the slight dependence of BV on T_{SJ} could be seen.

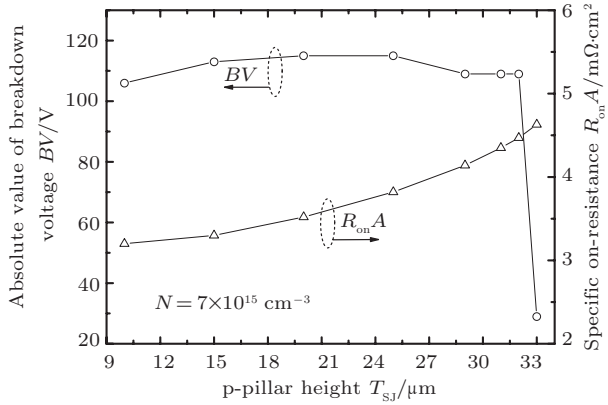


Fig. 11. The relationship of the breakdown voltage and the specific on-state resistance versus the p-pillar height for $N = 7\times10^{15}$ cm^{-3}.

In order to reveal the mechanism, Figure 12 shows the electric field distribution along the line A_1A_2 or B_1B_2, for three different T_{SJ} corresponding to Fig. 11. From Fig. 12, it could be seen that the shapes of all the electric field distributions almost do not change with the increasing T_{SJ}. These indicate quite a large part of the p-pillar regions and the n-pillar region could not play an effective role in sustaining the reverse voltage, and thus a low breakdown voltage.

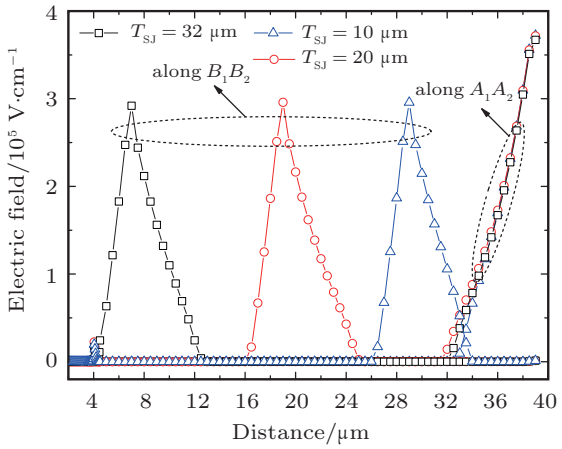


Fig. 12. (color online) Electric field distributions along the line A_1A_2 or B_1B_2 as shown in Fig. 1, for three different T_{SJ} in Fig. 11.

Aiming at the issue of the high n-drift concentration, an attempt of scaling down the dimension of the p-pillar and n-pillar widths is performed to improve the reverse blocking capability, as shown in Fig. 13. Thanks to the narrow pillar width

W_n of 5 μm, the variation laws of BV and $R_{on}A$ are similar to those in Fig. 9, with the peak absolute BV of 495 V and an $R_{on}A$ of 4.4 mΩ · cm^2 for $T_{SJ} = 31$ μm. This demonstrates it requires a narrower pillar width corresponding to a high N so as to achieve the good reverse blocking, which is consistent with the theory of SJ devices in the forward blocking applications.[2] As shown from Fig. 14, more uniform electric field distributions could be realized and thus a better reverse blocking.

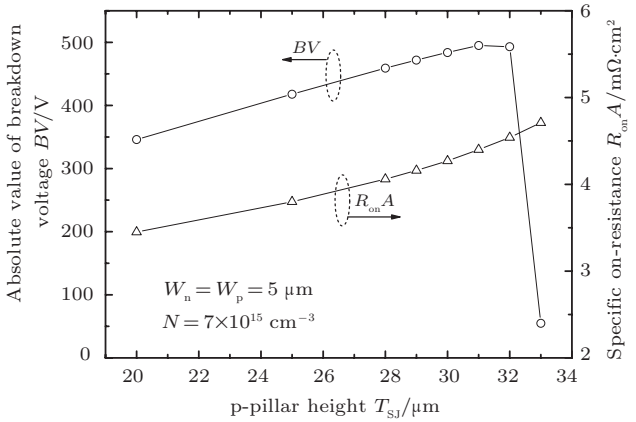


Fig. 13. The relationship of the breakdown voltage and the specific on-state resistance versus the p-pillar height for $N = 7 \times 10^{15}$ cm^{-3}. $W_n = W_p =$ 5 μm.

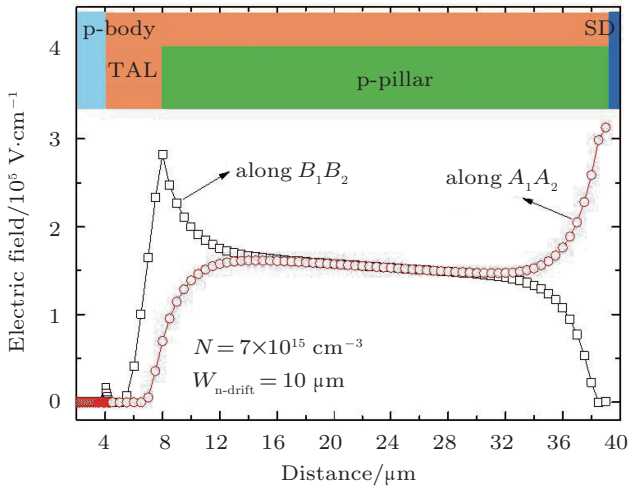


Fig. 14. (color online) Electric field distributions along the line A_1A_2 or B_1B_2 as shown in Fig. 1, for $BV = -495$ V, $T_{SJ} = 31$ μm, and $W_n = W_p =$ 5 μm corresponding to Fig. 13.

5. Trade-off property between $R_{on}A$ and BV

The trade-off characteristics of $R_{on}A$–BV for different MOSFETs are shown in Fig. 15. The trade-off characteristics for the VDMOS and the SJ MOSFET are related to the forward blocking while others for the reverse blocking. In the figure, the relationship of $R_{on}A$–BV with different N is obtained by optimizing T_{SJ} for the maximum absolute BV when $L = 35$ μm and $W_n = 8$ μm (or $W_n = 5$ μm). And it could be seen that there exists a proper range of N (2×10^{15} cm^{-3} ~ 5×10^{15} cm^{-3} for $W_n = 8$ μm, or 5×10^{15} cm^{-3} ~ 8×10^{15} cm^{-3} for $W_n = 5$ μm), in which a better trade-off could be obtained in the SD-D-semi-SJ MOSFET compared to the prediction of the SJ MOSFETs with the same W_n. And for a given N in this range, $N = 3 \times 10^{15}$ cm^{-3} and $N = 7 \times 10^{15}$ cm^{-3} for example, the relationship of $R_{on}A$–BV with different L, obtained by optimizing T_{SJ} for the maximum reverse BV, also exhibits a better trade-off compared to the conventional SJ MOSFET. Based on this, an interesting and useful rule, namely almost the same T_{TAL} could be used to obtain the maximum reverse BV with a low $R_{on}A$ for different L when N and W_n are constant, as illustrated in Table 2. According to this rule, it is easy to design an SD-D-semi-SJ MOSFET for the desired BV by only varying the T_{SJ}. In addition, as shown in the table, for a given BV, the improvement of the trade-off for a higher doping concentration could also be realized by decreasing p-pillar width from 8 μm to 5 μm, which is in agreement with the similar results of the forward blocking performance in the SJ MOSFETs.[12]

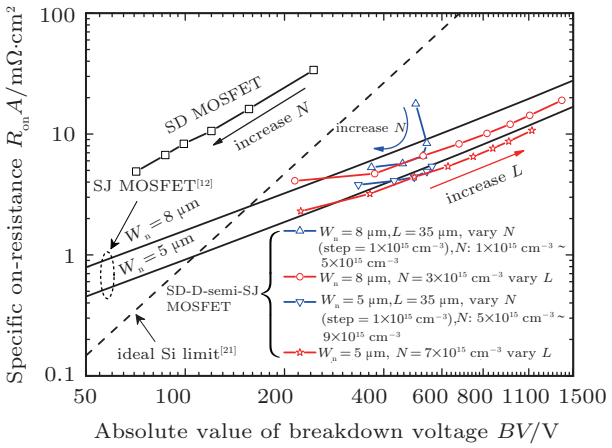


Fig. 15. (color online) The trade-off characteristics between the specific on-resistance and the breakdown voltage for different MOSFETs.

Table 2. Optimized values for the SD-D-semi-SJ MOSFET corresponding to Fig. 15.

L/μm	$N = 3 \times 10^{15}$ cm^{-3}			$N = 7 \times 10^{15}$ cm^{-3}		
	$W_n = 8$ μm			$W_n = 5$μm		
	T_{SJ}/μm	BV/V	$R_{on}A$/mΩ · cm^2	T_{SJ}/μm	BV/V	$R_{on}A$/mΩ · cm^2
35	7	526	6.6	4	495	4.4
45	7	676	8.3	4	626	5.4
55	7	822	10.1	4	747	6.5
65	7	966	12.1	4	857	7.6
75	7	1108	14.3	4	957	8.7
95	7	1386	19	4	1125	10.7

6. Fabrication issues

The main fabrication of our proposed SD-D-semi-SJ MOSFET is compatible with existing SJ MOSFET processes. The metal with relative high workfunction compared to the electron affinity of silicon, such as Cu, Ni, W, Ag or Pt, should be utilized to form the Schottky–drain.

7. Conclusions

In this paper, attempts to improve the reverse blocking capacity in vertical MOSFET with Schottky–drain and Schottky–drain-connected semisuperjunctions are performed for the first time. A novel device, the SD-D-semi-SJ MOSFET, is proposed and studied, with emphasis on the comparative analyses of device physical mechanisms. Compared with other counterparts and even the conventional SJ MOSFET of forward applications, the proposed device could realize not only the excellent reverse blocking ability but also the extremely low specific on-resistance. The improvement of the breakdown voltage benefits from the Schottky–drain contact and the SD-contacted-semisuperjunction, and the decrease of the specific on-resistance is due to the bipolar carrier transport properties of the p-pillar. A valuable design rule that only the SJ thickness needs determining to achieve the desired *BV* for a given doping concentration and pillar width, is extracted. These results demonstrate a significant superiority and a great potential of the SD-D-semi-SJ MOSFET in the reverse applications and may be of significance in the design of this device.

References

[1] Chen X B 1993 U.S. Patent 5 216 275

[2] Fujihira T 1997 *Jpn. J. Appl. Phys.* **36** 6254

[3] Saito W, Omura I, Aida S, Koduki S, Izumisawa M and Ogura T 2003 *IEEE Trans. Electron Dev.* **50** 1801

[4] Srikanth S and Karmalkar S 2008 *IEEE Trans. Electron Dev.* **55** 3562

[5] Ye H and Haldar P 2008 *IEEE Trans. Electron Dev.* **55** 2246

[6] Chen Y, Liang Y C, Samudra G S, Yang X, Buddharaju K D and Feng H H 2008 *IEEE Trans. Electron Dev.* **55** 211

[7] Napoli E, Wang H and Udrea F 2008 *IEEE Electron Dev. Lett.* **29** 249

[8] Tamaki T, Nakazawa Y, Kanai H, Abiko Y, Ikegami Y, Ishikawa M, Wakimoto E, Yasuda T and Eguchi S 2011 *Proceedings of the* 23*rd International Symosium on Power Semiconductor Devices and ICs*, May, 2011, San Diego, CA, USA, pp. 308–311

[9] Huang H M and Chen X B 2013 *IEEE Trans. Electron Dev.* **60** 1195

[10] Lyu X J and Chen X B 2013 *IEEE Trans. Electron Dev.* **60** 1709

[11] Lin Z, Huang H M and Chen X B 2015 *IEEE Trans. Electron Dev.* **62** 228

[12] Zhang W T, Zhang B, Li Z H, Qiao M and Li Z J 2015 *IEEE Trans. Electron Dev.* **62** 4114

[13] Murari B, Bertotti F and Vignola G A 2002 *Smart Power ICs*, 2nd edn. pp. 184–88

[14] Leberer R, Reber R and Oppermann M 2008 *IEEE MTT-S International Microwave Symposium Digest*, June 15–20, 2008, Atlanta, GA, p. 85

[15] Huang W and Chow T P 2007 *Proceedings of the* 19*th Inernational Symposium on Power Semiconductor Devices and ICs*, pp. 265–268

[16] Nagai S, Yamada Y, Negoro N, Handa H, Hiraiwa M, Otsuka N and Ueda D 2015 *IEEE Journal of the Electron Devices Society* **3** 7

[17] Bahat-Treidel E, Lossy R, Wurfl J and Trankle G 2009 *IEEE Electron Dev. Lett.* **30** 901

[18] Zhou C H, Chen W, Piner E L and Chen K J 2010 *IEEE Electron Dev. Lett.* **31** 668

[19] Zhao S L, Mi M H, Hou B, Luo J, Wang Y, Dai Y, Zhang J C, Ma X H and Hao Y 2014 *Chin. Phys. B* **23** 107303

[20] Atlas User's Manual 2015, Silvaco, Inc., Santa Clara, CA USA

[21] Hu C 1979 *IEEE Trans. Electron Dev.* **26** 243